Supplementary Material

for Cross-modal Active Complementary Learning with Self-refining Correspondence

Yang Qin[1], **Yuan Sun**[1], **Dezhong Peng**[1,3,4], **Joey Tianyi Zhou**[2],
Xi Peng[1], **Peng Hu**[1]*
[1] College of Computer Science, Sichuan University, Chengdu, China.
[2] Centre for Frontier AI Research (CFAR) and Institute of High
Performance Computing (IHPC), A*STAR, Singapore.
[3] Chengdu Ruibei Yingte Information Technology Co., Ltd, Chengdu, China.
[4] Sichuan Zhiqian Technology Co., Ltd, Chengdu, China.
`{qinyang.gm,joey.tianyi.zhou,pengx.gm,penghu.ml}@gmail.com,`
`sunyuan_work@163.com, pengdz@scu.edu.cn`

In this supplementary material, we provide additional information for CRCL. Specifically, we first give detailed proofs of Equation (1) and Lemma 1 in Appendix A. To improve the reproducibility of CRCL, in Appendix B, we provide comprehensive implementation details of our CRCL for different extended baselines (*i.e.*, VSE∞[1], SAF[2], and SGR[2]) on three datasets. In addition, we present richer additional experimental results and analysis in Appendix C, including parameter analysis, progressive analysis, and extra comparison results, to fully verify the effectiveness and superiority of CRCL. Finally, we supplemented related work in Appendix D to further discuss the related research background.

A Detailed Proofs

A.1 Proof for Equation (1)

$$C \leq R_{\mathcal{L}_r}(f^*) - R_{\mathcal{L}_r}(f^*_\eta) \leq 0, \tag{1}$$

where $C = 2\eta(A_{\min}^{(1-q)} - A_{\max}^{(1-q)})/(1 - \frac{N\eta}{N-1}) \leq 0$. C increases as q increases and when $q = 1$, C takes the maximum value 0. $A_{\min}$ and $A_{\max}$ are the maximum and minimum values of $\sum_{j=1}^{N} \tan(p_{ij})$ under the condition $\sum_{j=1}^{N} p_{ij} = 1$, where $1 < A_{\min} < A_{\max}$, and $0 \leq p_{ij} \leq 1$ ($p_{ij} = p_{ij}^{\circ}$ or $p_{ij}^{\diamond}$). f^* and f^*_η are the global minimizers of $R_{\mathcal{L}_r}(f)$ and $R^{\eta}_{\mathcal{L}_r}(f)$, respectively.

Proof. Recall that for any f,

$$\begin{aligned} R_{\mathcal{L}_r}(f) =& R_{\mathcal{L}_r^{\diamond}}(f) + R_{\mathcal{L}_r^{\circ}}(f) \\ =& \mathbb{E}_{(I_i,T_\cdot)\sim\mathcal{D}}\left[y_{i\cdot}\mathcal{L}_r^{\circ}(I_i, T_\cdot, q)\right] + \mathbb{E}_{(I_\cdot,T_i)\sim\mathcal{D}}\left[y_{\cdot i}\mathcal{L}_r^{\diamond}(T_i, I_\cdot, q)\right]. \\ =& \mathbb{E}_{(I_i,T_i)\sim\mathcal{D}}\left[\mathcal{L}_r^{\circ}(I_i, T_i, q)\right] + \mathbb{E}_{(I_i,T_i)\sim\mathcal{D}}\left[\mathcal{L}_r^{\diamond}(T_i, I_i, q)\right] \end{aligned}$$

[*] Corresponding author.

37th Conference on Neural Information Processing Systems (NeurIPS 2023).

For uniform noisy correspondence with noise rate η, we consider the image-to-text direction and have

$$\begin{aligned}
R^{\eta}_{\mathcal{L}_r^{\circ}}(f) =&\mathbb{E}_{(I_i,T.)\sim\mathcal{D}_\eta}\left[\tilde{y}_{i.}\mathcal{L}_r^{\circ}(I_i,T.,q)\right] \\
=&\mathbb{E}_{(I_i,T.)\sim\mathcal{D}}\left[(1-\eta)\mathcal{L}_r^{\circ}(I_i,T_i,q)+\frac{\eta}{N-1}\sum_{j\neq i}\mathcal{L}_r^{\circ}(I_i,T_j,q)\right] \\
=&\mathbb{E}_{(I_i,T.)\sim\mathcal{D}}\left[(1-\eta)\mathcal{L}_r^{\circ}(I_i,T_i,q)+\frac{\eta}{N-1}\Big((N-1)\triangle^{(1-q)}-\mathcal{L}_r^{\circ}(I_i,T_i,q)\Big)\right] \\
=&\mathbb{E}_{(I_i,T.)\sim\mathcal{D}}\left[(1-\frac{N\eta}{N-1})\mathcal{L}_r^{\circ}(I_i,T_i,q)+\eta\triangle^{(1-q)}\right],
\end{aligned}$$

where $\triangle=\sum\limits_{j=1}^{N}\tan(p^{\circ}_{ij})>1$. Since $\triangle$ has the maximum and minimum values ($A_{\min}$ and $A_{\max}$, we provide a solution in **Remark**.) under the condition $\sum_{j=1}^{N}p^{\circ}_{ij}=1, 0\leq p^{\circ}_{ij}\leq 1$, for any p°_{ij}, we have

$$(1-\frac{N\eta}{N-1})R_{\mathcal{L}_r^{\circ}}(f)+\eta A_{\min}^{(1-q)}\leq R^{\eta}_{\mathcal{L}_r^{\circ}}(f)\leq(1-\frac{N\eta}{N-1})R_{\mathcal{L}_r^{\circ}}(f)+\eta A_{\max}^{(1-q)}.$$

Similarly, the above equation also holds for $R_{\mathcal{L}_r^{\diamond}}(f)$ and $R^{\eta}_{\mathcal{L}_r^{\diamond}}(f)$, *i.e.*,

$$(1-\frac{N\eta}{N-1})R_{\mathcal{L}_r^{\diamond}}(f)+\eta A_{\min}^{(1-q)}\leq R^{\eta}_{\mathcal{L}_r^{\diamond}}(f)\leq(1-\frac{N\eta}{N-1})R_{\mathcal{L}_r^{\diamond}}(f)+\eta A_{\max}^{(1-q)}.$$

Thus, for $R^{\eta}_{\mathcal{L}_r}(f)$ and $R_{\mathcal{L}_r}(f)$, under $\eta\leq\frac{N-1}{N}$, we have

$$(1-\frac{N\eta}{N-1})R_{\mathcal{L}r}(f)+2\eta A_{\min}^{(1-q)}\leq R^{\eta}_{\mathcal{L}r}(f)\leq(1-\frac{N\eta}{N-1})R_{\mathcal{L}r}(f)+2\eta A_{\max}^{(1-q)}.$$

or equivalently,

$$(R^{\eta}_{\mathcal{L}r}(f)-2\eta A_{\max}^{(1-q)})/(1-\frac{N\eta}{N-1})\leq R_{\mathcal{L}r}(f)\leq(R^{\eta}_{\mathcal{L}r}(f)-2\eta A_{\min}^{(1-q)})/(1-\frac{N\eta}{N-1}).$$

Thus, for f^*_η,

$$R_{\mathcal{L}_r}(f^*)-R_{\mathcal{L}_r}(f^*_\eta)\geq(R^{\eta}_{\mathcal{L}_r}(f^*)-R^{\eta}_{\mathcal{L}_r}(f^*_\eta))/(1-\frac{N\eta}{N-1})+C\geq C, \tag{2}$$

or equivalently,

$$R^{\eta}_{\mathcal{L}_r}(f^*)-R^{\eta}_{\mathcal{L}_r}(f^*_\eta)\leq(1-\frac{N\eta}{N-1})(R_{\mathcal{L}_r}(f^*)-R_{\mathcal{L}_r}(f^*_\eta))+C'\leq C', \tag{3}$$

where $C=2\eta(A_{\min}^{(1-q)}-A_{\max}^{(1-q)})/(1-\frac{N\eta}{N-1})\leq 0$, $C'=2\eta(A_{\max}^{(1-q)}-A_{\min}^{(1-q)})\geq 0$, f^* is a minimizer of $R_{\mathcal{L}_r}(f)$. Since f^*_η and f^* are the minimizers of $R^{\eta}_{\mathcal{L}_r}(f)$ and $R_{\mathcal{L}_r}(f)$, respectively, we have $R^{\eta}_{\mathcal{L}_r}(f^*)-R^{\eta}_{\mathcal{L}_r}(f^*_\eta)\geq 0$ or $R_{\mathcal{L}_r}(f^*)-R_{\mathcal{L}_r}(f^*_\eta)\leq 0$. Besides, it can be seen from Figure 1 that C/C' increases/decreases as q increases. In other words, under $\eta\leq\frac{N-1}{N}$, the larger q is, the tighter the bound of Equation (3)/Equation (2) is. When q is 1, then $R_{\mathcal{L}_r}(f^*)=R_{\mathcal{L}_r}(f^*_\eta)$ or $R^{\eta}_{\mathcal{L}_r}(f^*)=R^{\eta}_{\mathcal{L}_r}(f^*_\eta)$. This completes the proof.

Remark For the maximum value of $\sum_{j=1}^{N}\tan(p_{ij})$, For brevity, let $y=\sum_{j=1}^{N}\tan(p_{ij})=\sum_{j=1}^{N}\tan(x_j)$ under the condition $\sum_{j=1}^{N}x_j=1$ and $0\leq x_j\leq 1$. For any $x_i,x_j\in[0,1]$, we have

$$\tan(x_i+x_j)=\frac{\tan(x_i)+\tan(x_j)}{1-\tan(x_i)\tan(x_j)}.$$

Since $0\leq 1-\tan(x_i)\tan(x_j)\leq 1$, we have

$$\tan(x_i+x_j)\geq(1-\tan(x_i)\tan(x_j))\tan(x_i+x_j)=\tan(x_i)+\tan(x_j).$$

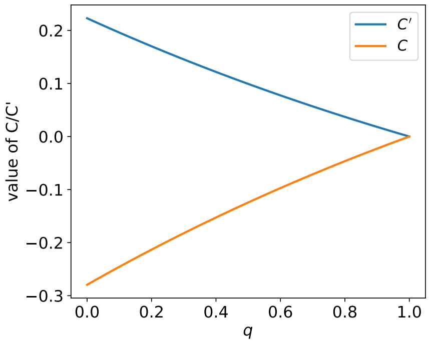

Figure 1: The value of C/C' changes with q, wherein N is 100 and η is 0.2.

Hence, $\sum_{j=1}^N \tan(x_j) \le \tan(\sum_{j=1}^N x_j) = \tan 1$, *i.e.*, $A_{max} = y_{max} = \tan 1 \approx 1.5574$.

For the minimum value of $y = \sum_{j=1}^N \tan(x_j)$, when $x_j \in (0,1)$, $\frac{\partial y}{\partial x_j} = \frac{1}{\cos^2 x_j} > 0$. Thus, the minimum value does not appear on the hyperplane boundary (0 or 1). We use the Lagrange Multiplier method [3] to construct the objective as follows

$$\min y, \ s.t. \sum_{j=1}^{N} x_j = 1 \Leftrightarrow \min_{x_j,\lambda}(y - \lambda(\sum_{j=1}^{N} x_j - 1)).$$

Let $f(x,\lambda) = y - \lambda(\sum_{j=1}^N x_j - 1) = \sum_{j=1}^N \tan(x_j) - \lambda(\sum_{j=1}^N x_j - 1)$, for x_j, λ, we have

$$\begin{cases} \frac{\partial f}{\partial x_j} = \frac{1}{\cos^2 x_j} - \lambda, & j = 1, 2, \cdots, N, \\ \frac{\partial f}{\partial \lambda} = \sum_{j=1}^N x_j - 1. \end{cases}$$

Let $\frac{\partial f}{\partial x_j} = \frac{\partial f}{\partial \lambda} = 0$, we have

$$\begin{cases} \lambda = \frac{1}{\cos^2 x_j}, & j = 1, 2, \cdots, N, \\ \sum_{j=1}^N x_j = 1. \end{cases}$$

Thus, when $x_1 = x_2 = \cdots = x_N = \frac{1}{N}$, y has a minimum value, *i.e.*, $A_{min} = y_{min} = N \tan \frac{1}{N}$>1.

□

A.2 Proof for Lemma 1

Lemma 1. *In an instance-level cross-modal matching problem, under uniform NC with noise rate* $\eta \le \frac{N-1}{N}$*, when* $q = 1$*,* $\mathcal{L}_r$ *is noise tolerant.*

Proof. Recall that for any f,

$$\begin{aligned} R_{\mathcal{L}_r}(f) =& R_{\mathcal{L}_r^\diamond}(f) + R_{\mathcal{L}_r^\circ}(f) \\ =& \mathbb{E}_{(I_i,T_\cdot)\sim\mathcal{D}}\left[y_{i\cdot}\mathcal{L}_r^\circ(I_i,T_\cdot,q)\right] + \mathbb{E}_{(I_\cdot,T_i)\sim\mathcal{D}}\left[y_{\cdot i}\mathcal{L}_r^\diamond(T_i,I_\cdot,q)\right]. \\ =& \mathbb{E}_{(I_i,T_i)\sim\mathcal{D}}\left[\mathcal{L}_r^\circ(I_i,T_i,q)\right] + \mathbb{E}_{(I_i,T_i)\sim\mathcal{D}}\left[\mathcal{L}_r^\diamond(T_i,I_i,q)\right] \end{aligned}$$

Under uniform noisy correspondence with noise rate η and $q = 1$, for any f, $R^{\eta}_{\mathcal{L}_r^{\circ}}(f)$ is written as

$$\begin{aligned} R^{\eta}_{\mathcal{L}_r^{\circ}}(f) =& \mathbb{E}_{(I_i,T_{\cdot})\sim\mathcal{D}_{\eta}}\left[\tilde{y}_{i\cdot}\mathcal{L}_r^{\circ}(I_i,T_{\cdot},q=1)\right] \\ =& \mathbb{E}_{(I_i,T_{\cdot})\sim\mathcal{D}}[(1-\eta)\mathcal{L}_r^{\circ}(I_i,T_i,q=1)+\frac{\eta}{N-1}\sum_{j\neq i}\mathcal{L}_r^{\circ}(I_i,T_j,q=1)] \\ =& \mathbb{E}_{(I_i,T_{\cdot})\sim\mathcal{D}}\left[(1-\eta)\mathcal{L}_r^{\circ}(I_i,T_i,q=1)+\frac{\eta}{N-1}\left((N-2)+\frac{\tan(p_{ii}^{\circ})}{\sum_{k=1}^{N}\tan(p_{ik}^{\circ})}\right)\right]- \quad (4) \\ =& \mathbb{E}_{(I_i,T_{\cdot})\sim\mathcal{D}}\left[(1-\eta)\mathcal{L}_r^{\circ}(I_i,T_i,q=1)+\frac{\eta}{N-1}\left((N-1)-\mathcal{L}_r^{\circ}(I_i,T_i,q=1)\right)\right] \\ =& (1-\frac{N\eta}{N-1})R_{\mathcal{L}_r^{\circ}}(f)+\eta \end{aligned}$$

Note that the equation between $R^{\eta}_{\mathcal{L}_r^{\diamond}}(f)$ and $R_{\mathcal{L}_r^{\diamond}}(f)$ can also be derived similarly as Equation (4), *i.e.*, $R^{\eta}_{\mathcal{L}_r^{\diamond}} = (1-\frac{N\eta}{N-1})R_{\mathcal{L}_r^{\diamond}}(f)+\eta$. Thus,

$$R^{\eta}_{\mathcal{L}_r}(f) = (1-\frac{N\eta}{N-1})R_{\mathcal{L}_r}(f)+2\eta$$

Now, for any f, $R^{\eta}_{\mathcal{L}_r}(f^*) - R^{\eta}_{\mathcal{L}_r}(f) = (1-\frac{N\eta}{N-1})(R_{\mathcal{L}_r}(f^*) - R_{\mathcal{L}_r}(f)) \leq 0$, where $\eta \leq \frac{N-1}{N}$ and f^* is a globalminimizer of $R_{\mathcal{L}_r}(f)$. This proves f^* is also the global minimizer of $R^{\eta}_{\mathcal{L}_r}(f)$. □

B Implementation Details

B.1 Model Settings

In this section, we mainly detail the model settings and the implementation of CRCL. To comprehensively verify the effectiveness of our framework, we apply our CRCL to VSE∞ [1], SAF [2], and SGR [2] for further robustness against NC, *i.e.*, CRCL-VSE∞, CRCL-SAF, and CRCL-SGR. For the VSE model used in our CRCL-VSE∞, we use the same encoder models as VSE∞ [1] to project the local region features and word embeddings into the shared common space and then utilize GPO [1] to aggregate local representations into global representations, wherein the dimensionality of the common space is 1024. For the CRCL-SAF/SGR, like DECL [4], we directly perform our CRCL on the similarity output of these models without any changes to their models. In all experiments, we use the same image region features and text backbone for fairness. More specifically, we utilize a Faster R-CNN detection model [5] to extract local-level BUTD features of salient regions with top-36 confidence scores for each image, like [6, 2]. These features are encoded into a 2,048-dimensional feature vector and then projected into 1,024-dimensional image representations in the common space. For each text, the Bi-GRU language backbone encodes the word tokens into the same dimensional semantic vector space as the image representation. Following [1], we employ the size augmentation on the training data, which is then fed into the model. For all parameter settings, see Appendix B.2. The code of our CRCL will be released on GitHub.

B.2 Parameter Settings

In this section, we fully provide the parameter settings of our experiments in Table 1 for easy reproducibility on three benchmark datasets, *i.e.*, Flickr30K, MS-COCO, and CC152K. We divide the parameter settings into two groups, the first group includes the parameter settings for the training without synthetic noise (=0%). The second group consists of the parameter settings for the training under synthetic noise ($> 0\%$). Simultaneously, each group details the training parameters of the three extensions of the baselines, *i.e.*, CRCL-VSE∞, CRCL-SAF, and CRCL-SGR. Note that the result of CRCL-SGRAF in the paper is the ensemble results of CRCL-SAF and CRCL-SGR. Following [2, 4, 7], the ensemble strategy is averaging the similarities computed by the two models and then performing image-text matching. Next, we will describe these main parameters. e_f represents the number of epochs to freeze the correspondence label, avoiding insufficient model training in the early stage from affecting the correction quality. e_i in $[e_1, \cdots, e_m]$ is the number of training epochs for the i-th SR piece. During the last SR piece, CRCL decays the learning rate (lr_rate) by 0.1 in lr_update epochs. τ and λ are the temperature parameter and the scale factor in ACL loss, respectively. β and ϵ are the momentum coefficient and the similarity threshold in SCC, respectively. For the parametric analysis of some hyper-parameters, see Appendix C.2 for more details.

Table 1: The settings of some key parameters for training on three datasets.

Noise	Datasets	Methods	e_f	$[e_1, \cdots, e_m]$	lr_update	lr_rate	β	τ	λ	ϵ
Synthetic noise $= 0\%$	CC152K	CRCL-VSE∞	2	[7,7,7,32]	17	0.0005	0.8	0.05	5	0.1
		CRCL-SAF	2	[7,7,7,42]	20	0.0005	0.8	0.05	5	0.1
		CRCL-SGR	2	[7,7,7,42]	20	0.0005	0.8	0.05	5	0.1
	Flickr30K	CRCL-VSE∞	2	[7,7,7,32]	15	0.0005	0.8	0.05	5	0.1
		CRCL-SAF	2	[7,7,7,32]	15	0.0005	0.8	0.05	5	0.1
		CRCL-SGR	2	[7,7,7,32]	15	0.0005	0.8	0.05	5	0.1
	MS-COCO	CRCL-VSE∞	2	[4,4,4,22]	12	0.0005	0.8	0.05	5	0.1
		CRCL-SAF	2	[4,4,4,22]	12	0.0005	0.8	0.05	5	0.1
		CRCL-SGR	2	[4,4,4,22]	12	0.0005	0.8	0.05	5	0.1
Synthetic noise $> 0\%$	Flickr30K	CRCL-VSE∞	2	[7,7,7,32]	15	0.0005	0.8	0.05	5	0.1
		CRCL-SAF	2	[7,7,7,32]	15	0.0005	0.8	0.05	5	0.1
		CRCL-SGR	2	[7,7,7,32]	15	0.0005	0.8	0.05	5	0.1
	MS-COCO	CRCL-VSE∞	2	[4,4,4,22]	12	0.0005	0.8	0.05	5	0.1
		CRCL-SAF	2	[4,4,4,22]	12	0.0005	0.8	0.05	5	0.1
		CRCL-SGR	2	[4,4,4,22]	12	0.0005	0.8	0.05	5	0.1

C Additional Experiments and Analysis

C.1 Parametric Analysis

The proposed CRCL has three sensitive key hyper-parameters, *i.e.*, the temperature parameter τ, the momentum coefficient β, and the similarity threshold ϵ. Thus, we conduct detailed parameter experiments (shown in Figure 2) on the Flickr30K dataset to evaluate the impact of different hyper-parameter settings and obtain better parameter settings for CRCL. Note that all parametric experiments are performed by CRCL-VSE∞ under 60% noise. As can be seen from Figure 2a, too large or too small τ both cause a performance drop. Thus, in all experiments, we recommend the range of τ is 0.03 $\sim$ 0.07. From Figure 2b, when the value of β is set to two extreme values, *i.e.*, 0 and 1, the performance drops remarkably. Moreover, in the range of $(0, 1)$, as β increases, the performance gradually improves. We think that with the increase of β, each correction performed by MC will retain more historical information to reduce perturbation. Thus providing more stable corrected correspondences for training. In all our experiments, β is 0.8. From Figure 2c, we can see that proper filtering is beneficial for mitigating NC. We think this filtering strategy can prevent the active loss from exploiting these confident noisy pairs to produce more misleading gradients. Thus, we set ϵ as 0.1 in all our experiments.

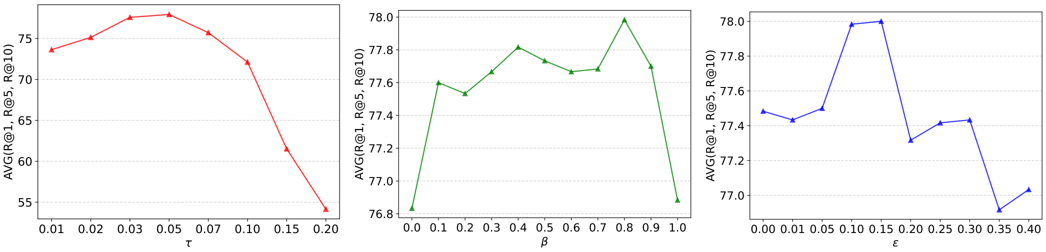

(a) The temperature parameter τ (b) The momentum coefficient β (c) The similarity threshold ϵ

Figure 2: Parametric analysis on Flickr30K with 60% noise.

C.2 Progressive Analysis

To comprehensively investigate the effectiveness of our CRCL, we carry out some progressive processes to further analyze the advantages of CRCL. Specifically, we recorded the performance of VSE∞ with different loss functions, including CRCL-VSE∞, $\mathcal{L}_d$, $\mathcal{L}_r(q = 1)$, $\mathcal{L}_r(q = 0)$, Complementary Contrastive Loss (CCL) [8], the hinge-based Triplet Ranking loss (TR) [9], the Triplet Tanking loss with Hard Negatives (TR-HN) [10], on Flickr30K under 80% noise. We visualize the performance of bidirectional retrieval in Figure 3. From the results, although $\mathcal{L}_r(q = 1)$ is noise-tolerant, which is consistent with the theoretical analysis (lemma 1), there would be some underfitting. Our CRCL with ACL loss fully explores the advantages of $\mathcal{L}_r$ and $\mathcal{L}_q$, showing remarkable robustness.

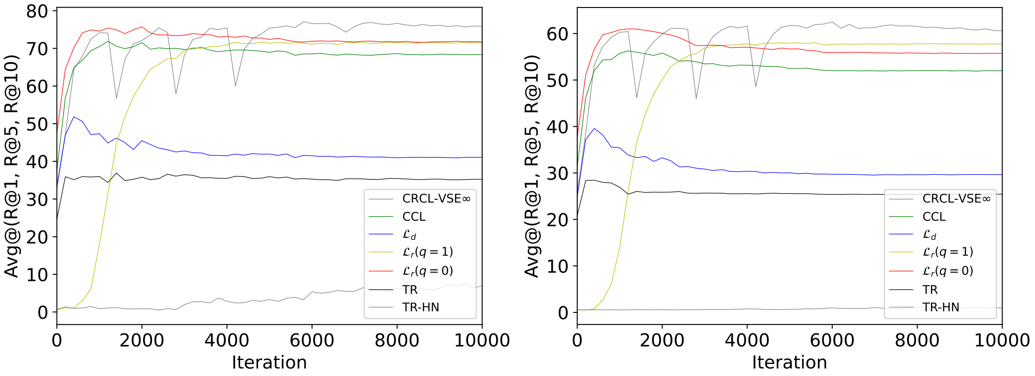

(a) Image-to-Text

(b) Text-to-Image

Figure 3: The performance of VSE∞ with different loss functions.

C.3 More Results under Synthetic Noisy Correspondences

To fully demonstrate the superiority and generalization of the proposed CRCL, we provide more comparison results under different robustness frameworks, including DECL[2] [4] and BiCro[3] [8]. In Table 2, except for the results of BiCro under 20%, 40%, and 60%, all other results are reproduced by us. From the results, our CRCL can significantly improve the robustness of existing methods (*e.g.*, VSE∞, SAF, and SGR) and outperform other advanced robust frameworks. It is worth noting that CRCL is also stable and superior in high noise, which shows the effectiveness of our CRCL.

C.4 More Results under Well-annotated Correspondences

In this section, we supplement the experimental results under well-annotated correspondences for a comprehensive and faithful comparison, including 17 state-of-the-art baselines, namely VSRN (ICCV'19) [11], CVSE (ECCV'20) [12], VSE∞ (CVPR'21) [1], MV-VSE (IJCAI'22) [13]; SCAN (ECCV'18) [6], CAMP (ICCV'19) [14], IMRAM (CVPR'20) [15], GSMN (CVPR'20) [16], SGRAF (AAAI'21) [2], NCR (NeurIPS'21) [17], DECL (ACM MM'22) [4], CGMN (TOMM'22) [18], URDA (TMM'22) [19], CMCAN (AAAI'22) [20], NAAF (CVPR'22) [21], CCR&CCS (WACV'23) [22], RCL (TPAMI'23) [8], and BiCro (CVPR'23) [7]. From the experimental results in Table 3, our CRCL achieves competitive results, which demonstrates the ability and potential of CRCL to handle well-correspondence scenarios.

D Related works

D.1 Image-Text Matching

Image-text matching methods mainly focus on learning latent visual-semantic relevance/similarities as the evidence for cross-modal retrieval [10, 6, 2, 1, 20, 23, 24, 25, 26, 27]. These approaches could be roughly classified into global- and local-level methods. To be specific, most global-level methods [10, 11, 1, 27] project images and texts into a shared global space, wherein cross-modal similarities could be computed [10, 1]. For example, Faghri et al. [10] proposed a triplet ranking

[2] `https://github.com/QinYang79/DECL`

[3] `https://github.com/xu5zhao/BiCro`

Table 2: Performance comparison (R@K(%) and rSum) of image-text retrieval on Flickr30K and MS-COCO 1K. The highest scores are shown in **bold**.

		Flickr30K							MS-COCO 1K						
		Image → Text			Text → Image				Image → Text			Text → Image			
Noise	Methods	R@1	R@5	R@10	R@1	R@5	R@10	rSum	R@1	R@5	R@10	R@1	R@5	R@10	rSum
20%	SAF	51.8	79.5	88.3	38.1	66.8	76.6	401.1	41.0	78.4	89.4	38.2	74.0	85.5	406.5
	SGR	61.2	84.3	91.5	44.5	72.1	80.2	433.8	49.1	83.8	92.7	42.5	77.7	88.2	434.0
	VSE∞	69.0	89.2	94.8	48.8	76.3	83.8	461.9	73.5	93.3	97.0	57.4	86.5	92.8	500.5
	DECL-SAF	73.1	93.0	96.2	57.0	82.0	88.4	489.7	77.2	**95.9**	98.4	61.6	89.0	95.3	517.4
	DECL-SGR	75.4	93.2	96.2	56.8	81.7	88.4	491.7	76.9	95.3	98.2	61.3	89.0	95.1	515.8
	BiCro-SAF	**77.0**	93.3	97.5	57.2	82.3	89.1	496.4	74.5	95.0	98.2	60.7	89.0	95.0	512.4
	BiCro-SGR	76.5	93.1	97.4	58.1	82.4	88.5	496.0	75.7	95.1	98.1	60.5	88.6	94.7	512.7
	CRCL-VSE∞	74.8	92.8	96.5	55.1	81.8	88.7	489.7	76.2	95.5	**98.6**	61.3	89.7	95.6	516.9
	CRCL-SAF	74.7	93.7	97.7	57.9	82.8	89.2	496.0	78.5	95.7	98.5	63.1	89.9	95.5	521.2
	CRCL-SGR	75.8	**94.6**	**97.6**	**59.1**	**84.0**	**90.1**	**501.2**	**78.9**	95.7	98.3	**63.6**	**90.3**	**95.7**	**522.5**
40%	SAF	34.3	65.6	78.4	30.1	58.0	68.5	334.9	36.0	74.4	87.0	33.7	69.4	82.5	383.0
	SGR	47.2	76.4	83.2	34.5	60.3	70.5	372.1	43.9	78.3	89.3	37.0	72.8	85.1	406.4
	VSE∞	30.2	58.3	70.2	22.3	49.6	62.7	293.3	53.3	84.3	92.1	31.4	63.8	75.0	399.9
	DECL-SAF	72.2	91.4	95.6	54.0	79.4	86.4	479.0	75.8	95.0	98.1	60.3	88.7	94.9	512.8
	DECL-SGR	72.4	92.2	96.5	54.5	80.1	87.1	482.8	75.9	95.3	98.2	60.2	88.3	94.8	512.7
	BiCro-SAF	72.5	91.7	95.3	53.6	79.0	86.4	478.5	75.2	95.0	97.9	59.4	87.9	94.3	509.7
	BiCro-SGR	72.8	91.5	94.6	54.7	79.0	86.3	478.9	74.6	94.8	97.7	59.4	87.5	94.0	508.0
	CRCL-VSE∞	71.2	92.6	96.3	53.2	80.4	87.4	481.1	74.4	95.1	**98.4**	59.5	89.1	95.2	511.7
	CRCL-SAF	74.2	93.8	97.1	57.0	81.8	88.6	492.5	76.4	**95.7**	98.1	**62.1**	89.3	95.3	516.9
	CRCL-SGR	**75.5**	**94.0**	**97.8**	**57.5**	**82.6**	**89.2**	**496.6**	**76.8**	95.3	98.2	61.9	**89.6**	**95.4**	**517.2**
60%	SAF	28.3	54.5	67.5	22.1	47.3	59.0	278.7	28.2	63.9	79.4	31.1	65.6	80.5	348.7
	SGR	28.7	58.0	71.0	23.8	49.5	60.7	291.7	37.6	73.3	86.3	33.8	68.6	81.7	381.3
	VSE∞	18.0	44.0	55.7	15.1	38.5	51.8	223.1	33.4	64.8	79.1	26.0	60.1	76.3	339.7
	DECL-SAF	66.4	88.1	93.6	49.8	76.1	84.4	458.4	71.1	93.6	97.3	57.9	86.8	93.8	500.5
	DECL-SGR	68.5	89.9	94.8	50.3	76.7	84.1	464.3	73.2	94.4	97.9	58.2	86.8	93.9	504.4
	BiCro-SAF	67.1	88.3	93.8	48.8	75.2	83.8	457.0	72.5	94.3	97.9	57.7	86.9	93.8	503.1
	BiCro-SGR	68.5	89.1	93.1	48.2	74.7	82.7	456.3	73.4	94.0	97.5	58.0	86.8	93.6	503.3
	CRCL-VSE∞	68.3	89.8	**95.9**	50.5	77.8	85.3	467.6	72.6	94.1	**98.0**	57.8	87.7	94.5	504.7
	CRCL-SAF	70.1	90.8	95.7	**53.0**	79.4	**86.9**	475.9	74.6	94.5	97.6	**59.5**	**88.3**	**94.7**	**509.2**
	CRCL-SGR	**70.5**	**91.3**	95.6	52.5	**79.4**	86.8	**476.1**	**74.6**	**94.6**	97.9	59.2	88.0	94.6	508.9
80%	SAF	12.2	32.8	48.4	11.8	30.5	41.5	177.2	24.2	57.5	74.1	24.7	57.1	73.0	310.6
	SGR	13.7	35.1	47.6	12.1	30.9	41.9	181.3	26.7	60.7	75.6	25.3	58.2	72.6	319.1
	VSE∞	8.1	23.1	34.7	7.4	22.6	31.8	127.7	25.4	55.1	70.6	19.2	50.5	68.0	288.8
	DECL-SAF	56.3	82.1	89.3	38.7	64.7	73.8	404.9	65.9	92.0	96.6	52.9	83.6	91.7	482.7
	DECL-SGR	55.1	79.8	87.2	37.4	63.4	72.9	395.8	65.6	91.6	96.6	52.0	83.0	91.3	480.1
	BiCro-SAF	2.4	9.1	15.8	2.4	8.3	13.7	51.7	39.6	72.6	84.7	22.4	52.8	67.1	368.9
	BiCro-SGR	1.7	8.7	13.7	1.3	5.1	8.9	39.4	31.4	62.0	75.2	30.0	60.7	73.2	332.5
	CRCL-VSE∞	55.3	82.1	89.1	39.7	68.2	77.8	412.2	67.9	92.8	**97.1**	53.1	84.7	92.5	488.1
	CRCL-SAF	58.4	83.9	90.5	**44.1**	70.7	79.8	427.4	**70.9**	92.8	**97.1**	55.2	85.3	92.9	494.2
	CRCL-SGR	**59.2**	**85.1**	**91.1**	43.6	**70.9**	**80.1**	**430.0**	70.7	**92.9**	**97.1**	**56.0**	**85.6**	**93.1**	**495.4**

loss with hard negatives to learn holistic visual-semantic embeddings for cross-modal retrieval. A Generalized Pooling Operator (GPO) [1] was proposed to adaptively aggregate different features (*e.g.*, region-based and grid-based ones) for better common representations. For the local-level methods, most of them desire to learn the latent fine-grained alignments across modalities for more accurate inference of visual-semantic relevance [6, 2, 20]. Representatively, Lee et al.[6] proposed a Stacked Cross Attention Network model (SCAN) to excavate the full latent alignments by contextualizing the image regions and word tokens for visual-semantic similarity inference. Diao et al. [2] proposed a Similarity Graph Reasoning and Attention Filtration model (SGRAF) for accurate cross-modal similarity inference by using a graph convolutional neural network for fine-grained alignments and an attention mechanism for representative alignments. Moreover, Zhang et al. [20] proposed a novel Cross-Modal Confidence-Aware Network to combine the confidence of matched region-word pairs with local semantic similarities for a more accurate visual-semantic relevance measurement. HREM [27] could explicitly capture both fragment-level relations within modality and instance-level relations across different modalities, leading to better retrieval performance. Pan et.al [26] propose a Cross-modal Hard Aligning Network (CHAN) to comprehensively exploit the most relevant region-word pairs and eliminate all other alignments, achieving better retrieval accuracy and efficiency. However, the aforementioned methods rely heavily on well-aligned image-text pairs while ignoring the inevitable noisy correspondences in data [17, 4], which will mislead the cross-modal learning and lead to performance corruption.

Table 3: Performance comparison (R@K(%) and rSum) of image-text retrieval on Flickr30K and MS-COCO 1K. The highest scores are shown in **bold**. * means global-level method.

	Flickr30K							MS-COCO 1K						
	Image → Text			Text → Image				Image → Text			Text → Image			
Methods	R@1	R@5	R@10	R@1	R@5	R@10	rSum	R@1	R@5	R@10	R@1	R@5	R@10	rSum
VSRN*	71.3	90.6	96.0	54.7	81.8	88.2	482.6	76.2	94.8	98.2	62.8	89.7	95.1	516.8
CVSE*	70.5	88.0	92.7	54.7	82.2	88.6	476.7	69.2	93.3	97.5	55.7	86.9	93.8	496.4
VSE∞*	76.5	94.2	97.7	56.4	83.4	89.9	498.1	78.5	96.0	98.7	61.7	90.3	95.6	520.8
MV-VSE*	79.0	94.9	97.7	59.1	84.6	90.6	505.9	78.7	95.7	98.7	62.7	90.4	95.7	521.9
SCAN	67.4	90.3	95.8	48.6	77.7	85.2	465.0	72.7	94.8	98.4	58.8	88.4	94.8	507.9
CAMP	68.1	89.7	95.2	51.5	77.1	85.3	466.9	72.3	94.8	98.3	58.5	87.9	95.0	506.8
IMRAM	74.1	93.0	96.6	53.9	79.4	87.2	484.2	76.7	95.6	98.5	61.7	89.1	95.0	516.6
GSMN	76.4	94.3	97.3	57.4	82.3	89.0	496.7	78.4	96.4	98.6	63.3	90.1	95.7	522.5
SGRAF	77.8	94.1	97.4	58.5	83.0	88.8	499.6	79.6	96.2	98.5	63.2	90.7	96.1	524.3
NCR	77.3	94.0	97.5	59.6	84.4	89.9	502.7	78.7	95.8	98.5	63.3	90.4	95.8	522.5
DECL	79.8	94.9	97.4	59.5	83.9	89.5	505.0	79.1	96.3	98.7	63.3	90.1	95.6	523.1
CGMN	77.9	93.8	96.8	59.9	85.1	90.6	504.1	76.8	95.4	98.3	63.8	90.7	95.7	520.7
UARDA	77.8	95.0	97.6	57.8	82.9	89.2	500.3	77.8	95.0	97.6	57.8	82.9	89.2	500.3
CMCAN	79.5	95.6	97.6	60.9	84.3	89.9	507.8	78.6	96.5	**98.9**	63.9	90.7	96.2	524.8
NAAF	78.3	94.1	97.7	58.9	83.3	89.0	501.3	78.9	96.0	98.7	63.1	**91.4**	**96.5**	524.6
CCR&CCS	79.3	95.2	98.0	59.8	83.6	88.8	504.7	80.2	**96.8**	98.7	64.3	90.6	95.8	526.4
RCL	79.9	**96.1**	97.8	61.1	85.4	90.3	510.6	80.4	96.4	98.7	64.3	90.8	96.0	526.6
BiCro	**80.7**	94.3	97.6	59.8	83.8	89.7	505.9	78.3	95.8	98.5	62.7	90.0	95.7	521.0
CRCL	78.5	95.5	**98.0**	**62.3**	**86.5**	**91.7**	**512.5**	**80.7**	96.5	98.6	**65.1**	91.2	96.1	**528.2**

D.2 Learning with Noisy Labels

Since the lack of well-annotated data in many real-world applications [28, 29, 30, 31, 32, 33, 34, 17], learning with incomplete/noisy supervision information is becoming more and more popular in recent years. In this section, we briefly review a few families of these methods against noisy labels: **1) Robust losses** aims to improve the robustness of loss functions to prevent models from overfitting on noisy labels [28, 35, 36, 37, 38, 30]. **2) Sample selection** [39, 40] mainly exploits the memorization effect of DNNs [41] to divide/select the corrupted samples from datasets, and then conduct different training strategies for clean and noisy data. **3) Correction Approaches**[42, 43, 44] attempt to correct the wrong supervision information (*e.g.*, labels or losses) for robust training through some ingenious mechanisms. Different from the aforementioned unimodal category-based methods, learning with noisy correspondence focuses on the noisy annotations existing across different modalities instead of classes [17, 4]. That is to say, noisy correspondences are instance-level noise instead of class-level noise, which is more challenging [17, 4]. To tackle this challenge, Huang et al. [17] first proposed a novel Noisy Correspondence Rectifier (NCR) to rectify the noisy correspondences with co-teaching. By introducing evidential deep learning into image-text matching, Qin et al. [4] proposed a general Deep Evidential Cross-modal Learning framework (DECL) to improve the robustness against noisy correspondences. Some recent works [8, 7] try to predict correspondence labels to recast the margin of triplet ranking loss [10] as a soft margin to further improve robustness like NCR, *e.g.*, cross-modal mete learning [8] and similarity-based consistency learning [7]. In addition to image-text matching, other fields are also troubled by NC, such as partially view-aligned clustering [45, 46, 47, 48], video-text retrieval [49], visible-infrared person re-identification [50]. In this paper, we mainly focus on the NC problem in image-text matching and try to address this from both robust loss function and correspondence correction.

References

[1] Jiacheng Chen, Hexiang Hu, Hao Wu, Yuning Jiang, and Changhu Wang. Learning the best pooling strategy for visual semantic embedding. In *Proceedings of the IEEE/CVF conference on computer vision and pattern recognition*, pages 15789–15798, 2021.

[2] Haiwen Diao, Ying Zhang, Lin Ma, and Huchuan Lu. Similarity reasoning and filtration for image-text matching. In *Proceedings of the AAAI Conference on Artificial Intelligence*, volume 35, pages 1218–1226, 2021.

[3] Dimitri P Bertsekas. *Constrained optimization and Lagrange multiplier methods*. Academic press, 2014.

[4] Yang Qin, Dezhong Peng, Xi Peng, Xu Wang, and Peng Hu. Deep evidential learning with noisy correspondence for cross-modal retrieval. In *Proceedings of the 30th ACM International Conference on Multimedia*, pages 4948–4956, 2022.

[5] Peter Anderson, Xiaodong He, Chris Buehler, Damien Teney, Mark Johnson, Stephen Gould, and Lei Zhang. Bottom-up and top-down attention for image captioning and visual question answering. In *Proceedings of the IEEE conference on computer vision and pattern recognition*, pages 6077–6086, 2018.

[6] Kuang-Huei Lee, Xi Chen, Gang Hua, Houdong Hu, and Xiaodong He. Stacked cross attention for image-text matching. In *Proceedings of the European conference on computer vision (ECCV)*, pages 201–216, 2018.

[7] Shuo Yang, Zhaopan Xu, Kai Wang, Yang You, Hongxun Yao, Tongliang Liu, and Min Xu. Bicro: Noisy correspondence rectification for multi-modality data via bi-directional cross-modal similarity consistency. *arXiv preprint arXiv:2303.12419*, 2023.

[8] Peng Hu, Zhenyu Huang, Dezhong Peng, Xu Wang, and Xi Peng. Cross-modal retrieval with partially mismatched pairs. *IEEE Transactions on Pattern Analysis and Machine Intelligence*, pages 1–15, 2023.

[9] Ryan Kiros, Ruslan Salakhutdinov, and Richard S Zemel. Unifying visual-semantic embeddings with multimodal neural language models. *arXiv preprint arXiv:1411.2539*, 2014.

[10] Fartash Faghri, David J Fleet, Jamie Ryan Kiros, and Sanja Fidler. Vse++: Improving visual-semantic embeddings with hard negatives. *arXiv preprint arXiv:1707.05612*, 2017.

[11] Kunpeng Li, Yulun Zhang, Kai Li, Yuanyuan Li, and Yun Fu. Visual semantic reasoning for image-text matching. In *Proceedings of the IEEE/CVF international conference on computer vision*, pages 4654–4662, 2019.

[12] Haoran Wang, Ying Zhang, Zhong Ji, Yanwei Pang, and Lin Ma. Consensus-aware visual-semantic embedding for image-text matching. In *Computer Vision–ECCV 2020: 16th European Conference, Glasgow, UK, August 23–28, 2020, Proceedings, Part XXIV 16*, pages 18–34. Springer, 2020.

[13] Zheng Li, Caili Guo, Zerun Feng, Jenq-Neng Hwang, and Xijun Xue. Multi-view visual semantic embedding. IJCAI, 2022.

[14] Zihao Wang, Xihui Liu, Hongsheng Li, Lu Sheng, Junjie Yan, Xiaogang Wang, and Jing Shao. Camp: Cross-modal adaptive message passing for text-image retrieval. In *Proceedings of the IEEE/CVF international conference on computer vision*, pages 5764–5773, 2019.

[15] Hui Chen, Guiguang Ding, Xudong Liu, Zijia Lin, Ji Liu, and Jungong Han. Imram: Iterative matching with recurrent attention memory for cross-modal image-text retrieval. In *Proceedings of the IEEE/CVF conference on computer vision and pattern recognition*, pages 12655–12663, 2020.

[16] Chunxiao Liu, Zhendong Mao, Tianzhu Zhang, Hongtao Xie, Bin Wang, and Yongdong Zhang. Graph structured network for image-text matching. In *Proceedings of the IEEE/CVF conference on computer vision and pattern recognition*, pages 10921–10930, 2020.

[17] Zhenyu Huang, Guocheng Niu, Xiao Liu, Wenbiao Ding, Xinyan Xiao, Hua Wu, and Xi Peng. Learning with noisy correspondence for cross-modal matching. *Advances in Neural Information Processing Systems*, 34:29406–29419, 2021.

[18] Yuhao Cheng, Xiaoguang Zhu, Jiuchao Qian, Fei Wen, and Peilin Liu. Cross-modal graph matching network for image-text retrieval. *ACM Transactions on Multimedia Computing, Communications, and Applications (TOMM)*, 18(4):1–23, 2022.

[19] Kunpeng Li, Yulun Zhang, Kai Li, Yuanyuan Li, and Yun Fu. Image-text embedding learning via visual and textual semantic reasoning. *IEEE Transactions on Pattern Analysis and Machine Intelligence*, 2022.

[20] Huatian Zhang, Zhendong Mao, Kun Zhang, and Yongdong Zhang. Show your faith: Cross-modal confidence-aware network for image-text matching. 2022.

[21] Kun Zhang, Zhendong Mao, Quan Wang, and Yongdong Zhang. Negative-aware attention framework for image-text matching. In *Proceedings of the IEEE/CVF Conference on Computer Vision and Pattern Recognition*, pages 15661–15670, 2022.

[22] Yuxiao Chen, Jianbo Yuan, Long Zhao, Tianlang Chen, Rui Luo, Larry Davis, and Dimitris N Metaxas. More than just attention: Improving cross-modal attentions with contrastive constraints for image-text matching. In *Proceedings of the IEEE/CVF Winter Conference on Applications of Computer Vision*, pages 4432–4440, 2023.

[23] Yang Liu, Hong Liu, Huaqiu Wang, and Mengyuan Liu. Regularizing visual semantic embedding with contrastive learning for image-text matching. *IEEE Signal Processing Letters*, 29:1332–1336, 2022.

[24] Yan Huang, Yuming Wang, Yunan Zeng, and Liang Wang. Mack: multimodal aligned conceptual knowledge for unpaired image-text matching. *Advances in Neural Information Processing Systems*, 35:7892–7904, 2022.

[25] Shashank Goel, Hritik Bansal, Sumit Bhatia, Ryan Rossi, Vishwa Vinay, and Aditya Grover. Cyclip: Cyclic contrastive language-image pretraining. *Advances in Neural Information Processing Systems*, 35:6704–6719, 2022.

[26] Zhengxin Pan, Fangyu Wu, and Bailing Zhang. Fine-grained image-text matching by cross-modal hard aligning network. In *Proceedings of the IEEE/CVF Conference on Computer Vision and Pattern Recognition*, pages 19275–19284, 2023.

[27] Zheren Fu, Zhendong Mao, Yan Song, and Yongdong Zhang. Learning semantic relationship among instances for image-text matching. In *Proceedings of the IEEE/CVF Conference on Computer Vision and Pattern Recognition*, pages 15159–15168, 2023.

[28] Aritra Ghosh, Himanshu Kumar, and P Shanti Sastry. Robust loss functions under label noise for deep neural networks. In *Proceedings of the AAAI conference on artificial intelligence*, volume 31, 2017.

[29] Yalan Qin, Chuan Qin, Xinpeng Zhang, Donglian Qi, and Guorui Feng. Nim-nets: Noise-aware incomplete multi-view learning networks. *IEEE Transactions on Image Processing*, 32:175–189, 2022.

[30] Yanglin Feng, Hongyuan Zhu, Dezhong Peng, Xi Peng, and Peng Hu. Rono: Robust discriminative learning with noisy labels for 2d-3d cross-modal retrieval. In *Proceedings of the IEEE/CVF Conference on Computer Vision and Pattern Recognition (CVPR)*, pages 11610–11619, June 2023.

[31] Yijie Lin, Mouxing Yang, Jun Yu, Peng Hu, Changqing Zhang, and Xi Peng. Graph matching with bi-level noisy correspondence. In *Proceedings of the IEEE/CVF international conference on computer vision*, 2023.

[32] Peng Hu, Xi Peng, Hongyuan Zhu, Liangli Zhen, and Jie Lin. Learning cross-modal retrieval with noisy labels. In *Proceedings of the IEEE/CVF Conference on Computer Vision and Pattern Recognition*, pages 5403–5413, 2021.

[33] Yalan Qin, Xinpeng Zhang, Liquan Shen, and Guorui Feng. Maximum block energy guided robust subspace clustering. *IEEE Transactions on Pattern Analysis and Machine Intelligence*, 45(2):2652–2659, 2022.

[34] Yalan Qin, Hanzhou Wu, Xinpeng Zhang, and Guorui Feng. Semi-supervised structured subspace learning for multi-view clustering. *IEEE Transactions on Image Processing*, 31:1–14, 2021.

[35] Zhilu Zhang and Mert Sabuncu. Generalized cross entropy loss for training deep neural networks with noisy labels. *Advances in neural information processing systems*, 31, 2018.

[36] Yilun Xu, Peng Cao, Yuqing Kong, and Yizhou Wang. L_dmi: A novel information-theoretic loss function for training deep nets robust to label noise. *Advances in neural information processing systems*, 32, 2019.

[37] Yisen Wang, Xingjun Ma, Zaiyi Chen, Yuan Luo, Jinfeng Yi, and James Bailey. Symmetric cross entropy for robust learning with noisy labels. In *Proceedings of the IEEE/CVF International Conference on Computer Vision*, pages 322–330, 2019.

[38] Xingjun Ma, Hanxun Huang, Yisen Wang, Simone Romano, Sarah Erfani, and James Bailey. Normalized loss functions for deep learning with noisy labels. In *International conference on machine learning*, pages 6543–6553. PMLR, 2020.

[39] Junnan Li, Richard Socher, and Steven CH Hoi. Dividemix: Learning with noisy labels as semi-supervised learning. *arXiv preprint arXiv:2002.07394*, 2020.

[40] Yangdi Lu, Yang Bo, and Wenbo He. An ensemble model for combating label noise. In *Proceedings of the Fifteenth ACM International Conference on Web Search and Data Mining*, pages 608–617, 2022.

[41] Devansh Arpit, Stanisław Jastrzębski, Nicolas Ballas, David Krueger, Emmanuel Bengio, Maxinder S. Kanwal, Tegan Maharaj, Asja Fischer, Aaron Courville, Yoshua Bengio, and Simon Lacoste-Julien. A closer look at memorization in deep networks. In Doina Precup and Yee Whye Teh, editors, *Proceedings of the 34th International Conference on Machine Learning*, volume 70 of *Proceedings of Machine Learning Research*, pages 233–242. PMLR, 06–11 Aug 2017.

[42] Giorgio Patrini, Alessandro Rozza, Aditya Krishna Menon, Richard Nock, and Lizhen Qu. Making deep neural networks robust to label noise: A loss correction approach. In *Proceedings of the IEEE conference on computer vision and pattern recognition*, pages 1944–1952, 2017.

[43] Daiki Tanaka, Daiki Ikami, Toshihiko Yamasaki, and Kiyoharu Aizawa. Joint optimization framework for learning with noisy labels. In *Proceedings of the IEEE conference on computer vision and pattern recognition*, pages 5552–5560, 2018.

[44] Yangdi Lu and Wenbo He. Selc: Self-ensemble label correction improves learning with noisy labels. In Lud De Raedt, editor, *Proceedings of the Thirty-First International Joint Conference on Artificial Intelligence, IJCAI-22*, pages 3278–3284. International Joint Conferences on Artificial Intelligence Organization, 7 2022. Main Track.

[45] Mouxing Yang, Yunfan Li, Peng Hu, Jinfeng Bai, Jiancheng Lv, and Xi Peng. Robust multi-view clustering with incomplete information. *IEEE Transactions on Pattern Analysis and Machine Intelligence*, 45(1):1055–1069, 2022.

[46] Mouxing Yang, Yunfan Li, Zhenyu Huang, Zitao Liu, Peng Hu, and Xi Peng. Partially view-aligned representation learning with noise-robust contrastive loss. In *Proceedings of the IEEE/CVF conference on computer vision and pattern recognition*, pages 1134–1143, 2021.

[47] Jie Wen, Chengliang Liu, Shijie Deng, Yicheng Liu, Lunke Fei, Ke Yan, and Yong Xu. Deep double incomplete multi-view multi-label learning with incomplete labels and missing views. *IEEE Transactions on Neural Networks and Learning Systems*, 2023.

[48] Xu Yang, Cheng Deng, Kun Wei, Junchi Yan, and Wei Liu. Adversarial learning for robust deep clustering. *Advances in Neural Information Processing Systems*, 33:9098–9108, 2020.

[49] Huaiwen Zhang, Yang Yang, Fan Qi, Shengsheng Qian, and Changsheng Xu. Robust video-text retrieval via noisy pair calibration. *IEEE Transactions on Multimedia*, 2023.

[50] Mouxing Yang, Zhenyu Huang, Peng Hu, Taihao Li, Jiancheng Lv, and Xi Peng. Learning with twin noisy labels for visible-infrared person re-identification. In *Proceedings of the IEEE/CVF Conference on Computer Vision and Pattern Recognition*, pages 14308–14317, 2022.